

OPTICAL FIBRES

PACS numbers: 42.81.Cn; 42.70.Qs
DOI: 10.1070/QE2010v040n06ABEH014328

Dispersion and guidance characteristics of microstructured $68TeO_2-22WO_3-8La_2O_3-2Bi_2O_3$ glass fibres for supercontinuum generation

Yu.P. Yatsenko, V.O. Nazaryants, A.F. Kosolapov, M.S. Astapovich, V.G. Plotnichenko, E.M. Dianov, A.N. Moiseev, M.F. Churbanov, V.V. Dorofeev, A.V. Chilyasov, G.E. Snopatin

Abstract. **We report the preparation of a high-purity optical-quality four-component glass of composition $68TeO_2-22WO_3-8La_2O_3-2Bi_2O_3$, containing $(2.7\pm0.5)\times10^{-5}$ mol% OH groups. Its refractive index has been determined in the range 0.9–5.45 μm using interference refractometry. The data are used to assess the dispersion and guidance characteristics of microstructured optical fibres potentially attractive for supercontinuum generation in the range 1–5 μm.**

Keywords: *tellurite glasses, microstructured optical fibres, supercontinuum generation.*

1. Introduction

In recent years, a great deal of attention has been paid to the mid-IR spectral region, primarily because mid-IR radiation has many potential applications in analytical spectroscopy since most chemical compounds have absorption bands in this range. Intense research effort is underway to create both efficient laser sources and advanced, low-loss optical materials. Significant progress has been made in the development of low-melting-point multicomponent (chalcogenide, fluoride and tellurite) glasses containing heavy metals and having low phonon energy and low mid-IR optical loss. Among the wide diversity of such glasses, considerable potential for optical fibre fabrication is offered by tellurite glasses, which have the advantages of stable composition, broadband transmission (0.35–6 μm) and large linear (n = 1.98–2.1) and nonlinear ($n_2 = (2.5-14.8)\times10^{-19}$ m^2 W^{-1}) refractive indices [1–10].

One of the most interesting applications for optical fibres fabricated from highly nonlinear tellurite glasses is mid-IR supercontinuum generation. Fibres for this application should as a rule have a sufficiently flat dispersion profile in their anomalous region and a dispersion zero sufficiently close (typically within 100 nm) to the pump wavelength.

Yu.P. Yatsenko, V.O. Nazaryants, A.F. Kosolapov, M.S. Astapovich, V.G. Plotnichenko, E.M. Dianov Fiber Optics Research Center, Russian Academy of Sciences, ul. Vavilova 38, 119333 Moscow, Russia; e-mail: yuriya@fo.gpi.ru, kaf@fo.gpi.ru;
A.N. Moiseev, M.F. Churbanov, V.V. Dorofeev, A.V. Chilyasov, G.E. Snopatin Institute of Chemistry of High-Purity Substances, Russian Academy of Sciences, ul. Tropinina 49, 603950 Nizhnii Novgorod, Russia

Received 30 March 2010; revision received 24 April 2010
Kvantovaya Elektronika **40** (6) 513–518 (2010)
Translated by O.M. Tsarev

The material dispersion zero of tellurite glasses ($\lambda_0 \sim 2.2$ μm) is rather far away from the output wavelengths of available femtosecond IR lasers, such as erbium (λ = 1.55 μm) or thulium ($\lambda \sim 2$ μm) lasers. To use such systems as pump sources for supercontinuum generation, microstructured fibre geometries are needed. The waveguide dispersion of microstructured fibres allows one to tune the shape of the dispersion curve in a wide range, in particular to shift the zero-dispersion point to shorter wavelengths.

Because the viscosity of tellurite glasses is a stronger function of temperature in comparison with silica-based glasses, the fabrication of microstructured tellurite fibres with complex structures presents more serious technical problems. Microstructured fibres made of tellurite glasses typically have only one ring of air holes. Only very recently have Liao et al. [8] demonstrated a tellurite fibre having four rings of holes. In the vast majority of studies microstructured fibres have been used for supercontinuum generation at a pump wavelength of 1.55 μm. The structure of fibres intended for pumping in the spectral range of the thulium laser (near 2 μm), which are potentially suitable for supercontinuum generation at longer wavelengths, has not yet been studied in sufficient detail.

Domachuk et al. [5] reported microstructured fibre made of $TeO_2-ZnO-PbO-PbF_2-Nb_2O_5$ tellurite glass. The 1.750-μm loss in the fibre was 8×10^3 dB km^{-1}. Nevertheless, the strong nonlinearity of the glass (nonlinear waveguide coefficient γ = 596 W^{-1} km^{-1}) the use of femtosecond pump pulses (T_{FWHM} = 110 fs) enabled supercontinuum generation in the range 0.789–4.870 μm at a fibre length under 1 cm. Lin et al. [6] used $80TeO_2-10ZnO-10Na_2O$ glass. Optimising the glass composition and using a multistage dehydration process, they were able to reduce the concentration of OH groups and produce fibre with an optical loss of 240–700 dB km^{-1} at 1.550 μm.

A major problem in the preparation of tellurite glasses is purification of the raw materials, in particular, the removal of OH groups – the main impurities absorbing in the range 2.5–5 μm [11].

In this paper, we report the preparation of a high-purity four-component glass of composition $68TeO_2-22WO_3-8La_2O_3-2Bi_2O_3$ with a record low level of OH groups, $(2.7\pm0.5)\times10^{-5}$ mol%, and a 45 dB km^{-1} absorption at 1.975 μm. The refractive index of the glass has been determined throughout its transmission window (0.9–5.45 μm) using interference refractometry, and dispersion and guidance characteristics have been numerically simulated for two microstructured fibre geometries attractive for supercontinuum generation in the range 1–5 μm.

2. Preparation of high-purity tellurite glass

$68TeO_2-22WO_3-8La_2O_3-2Bi_2O_3$ glass was prepared by melting a mixture of high-purity constituent oxides in a platinum crucible at 800 °C under flowing purified oxygen in a hermetically sealed fused-silica reactor. The starting chemicals used were tellurium dioxide and tungsten trioxide prepared at the Institute of Chemistry of High-Purity Substances, Russian Academy of Sciences (3d transition metal impurities each within 0.1 ppm by weight) and commercially available ultrapure lanthanum and bismuth oxides (3d transition metals within 1 ppm by weight).

The content of hydrocarbon impurities in the oxygen was below the detection limit of gas chromatography (below 0.01–0.05 mppm), and the water vapour content was within 0.5 mppm (dew point temperature from –90 to –80 °C).

After homogenisation, the melt was cast into preheated cylindrical quartz moulds 17 mm in inner diameter. The solidified material was annealed at the glass transition temperature and then slowly cooled. Next, the glass sample was withdrawn from the mould and subjected to mechanical processing. The OH content (C_{OH}) was determined by IR spectroscopy using the absorption band near 3 μm. The absorption coefficient of the glass was determined to be 0.001–0.0075 cm^{-1} (Fig. 1), which is three orders of magnitude below that of other tellurite glasses with roughly the same TeO_2 content [12, 13].

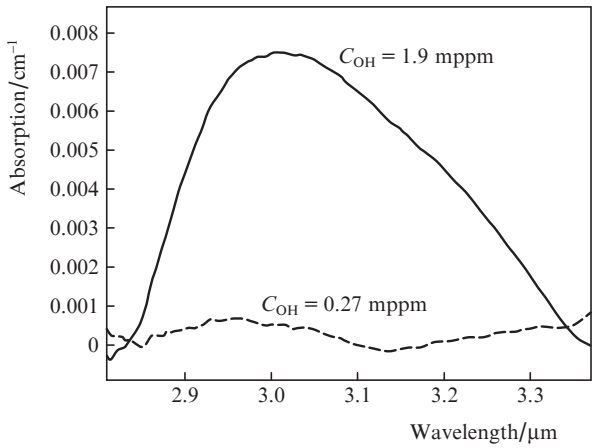

Figure 1. Absorption band of OH groups near 3 μm for tellurite glasses prepared by drying and melting the batch under flowing dry oxygen (solid curve) and using a chemical reagent (dashed curve).

Visual and polarised-light inspection showed that the glass was free of large striae. Microscopic examination revealed no inhomogeneities or scattering centres. The content of regulated 3d transition metal impurities (Cr, Cu, Mn, Fe, Ni, Co and V) was within the detection limits of direct atomic emission analysis and mass spectrometry (0.1–0.5 ppm by weight), except for Fe, which was present at a level of 0.3 ppm by weight. Platinum, originating from the crucible material, was present at a level of 1–10 ppm by weight. Phosphorus, an anion impurity, was detected by mass spectrometry at a level of 0.4 ppm by weight.

The volume absorption coefficient of the glass was measured at two wavelengths (1.560 and 1.975 μm) by laser calorimetry [14, 15] and was determined to be 76 and 45 dB km^{-1}, respectively.

3. Wavelength-dependent refractive index measurements

The refractive index of the glass was measured as a function of wavelength using a modified interference refractometry technique [16]. To this end, we prepared plane-parallel plates of three thicknesses (about 0.6, 1 and 1.5 μm), with optically polished faces. The sample thickness was measured with an accuracy of 0.05–0.1 μm using a DG-30 length gauge.

Interference transmission spectra of the samples were measured on a Bruker IFS-113v Fourier transform spectrometer in the range 1000–12000 cm^{-1} (0.8–10 μm) with a 0.1-cm^{-1} resolution. We also measured the transmission spectra of the samples in the range 0.35–3.3 μm on a PerkinElmer Lambda 900 spectrophotometer with a 4-nm resolution and determined the transmittance at 2.012, 1.340 and 1.090 μm. From the measured transmission spectra of the plates, we determined the frequency of interference peaks, ν_m, which were then used to determine the refractive index as

$$n_i(\nu_m) = \frac{m}{2h_i\nu_m}, \tag{1}$$

where $n_i(\nu_m)$ is the refractive index of sample i at frequency ν_m; h_i is the thickness of sample i; and m is the order of the peak corresponding to frequency ν_m. The order of the peaks was determined as

$$\frac{m_1}{m_2} - \frac{h_1}{h_2} = \text{const}. \tag{2}$$

The spectral dependence of the refractive index is presented in Fig. 2. The points represent the refractive index calculated from the absolute transmittances at 2.012, 1.340 and 1.090 μm, which were used as input approximations for calculating the refractive index from the position of the interference peaks. According to our estimates, the uncertainty in the refractive index obtained is 3×10^{-4}. The refractive indices calculated by Eqn (1) (more than 70000 values) were fitted to a generalised Cauchy dispersion formula of the eighth degree,

$$n(\lambda) = \sum_{i=2}^{8} A_i\lambda^i + C + \sum_{i=2}^{8} B_i\lambda^{-i} \tag{3}$$

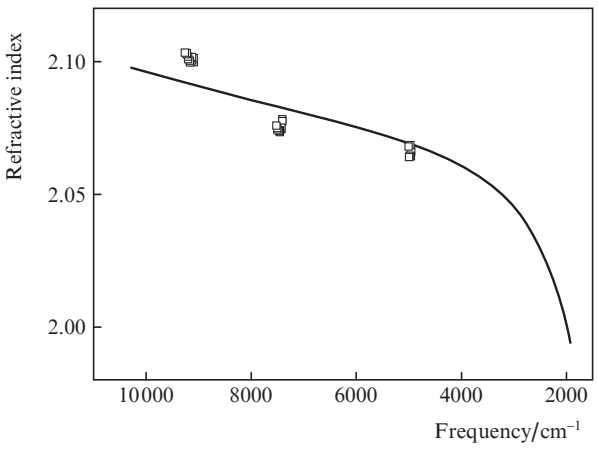

Figure 2. Spectral dependence of the refractive index for the tellurite glass.

Table 1. Best fit coefficients in (3).

Coefficient	Value
C	2.07416
A_2	-2.66140×10^{-3}
B_2	2.36742×10^{-2}
A_4	-1.14815×10^{-5}
B_4	1.09489×10^{-3}
A_6	6.70703×10^{-8}
B_6	-9.14458×10^{-5}
A_8	-3.49691×10^{-9}
B_8	5.73297×10^{-5}

over the entire range where the interference curve had been measured, 0.9 to 5.45 μm (coefficients A_i, B_i and C are given in Table 1).

The rms deviation of $n(\lambda)$ from the data points over the entire spectrum was 1×10^{-5}. The spectral dependences of the material dispersion and its slope for the tellurite glass studied were determined by differentiating (3). The zero material dispersion wavelength was found to be $\lambda_0 = 2.22$ μm.

4. Calculation of microstructured fibre parameters

The refractive index of the tellurite glass measured throughout its transmission window can be used to assess the guidance and dispersion characteristics of fibre for supercontinuum generation. We studied the characteristics of two simple microstructured tellurite fibre designs for supercontinuum generation under laser pumping near 2 μm. One of them (Fig. 3) has two rings of hexagonally arranged holes with a large hole diameter to pitch ratio: $d_{1,2}/\Lambda = 0.9$. The other has four rings of holes, with a relatively small $d_{1,2,3}/\Lambda$ (under 0.5) in the three inner rings and $d_4/\Lambda = 0.9$ in the fourth ring (Fig. 6).

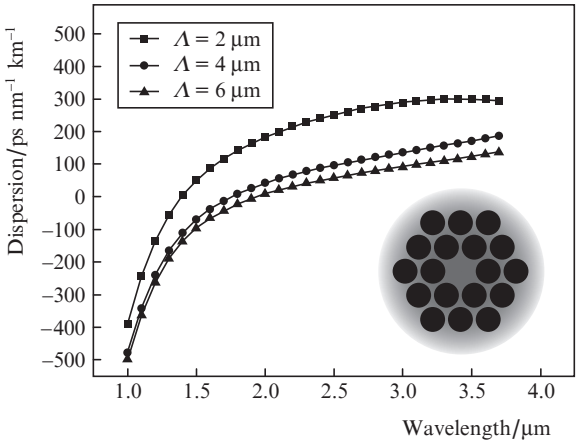

Figure 3. Dispersion profiles of two-ring microstructured $68TeO_2$–$22WO_3$–$8La_2O_3$–$2Bi_2O_3$ fibres with $d_{1,2}/\Lambda = 0.9$ and different hole pitches.

Their dispersion characteristics were calculated by the finite element method using the standard pack MATLAB 7.0–FEMLAB 3.1. To estimate the waveguiding loss, perfectly matched layers were introduced as boundary conditions. The effective refractive index of the fundamental mode was calculated using the spectral dependence of the refractive index (3) obtained in this study for the glass under consideration. In optimising the fibre geometry, the basic criteria were

– a zero dispersion wavelength in the range 1.8–2 μm and
– the minimum possible dispersion slope, effective mode area and waveguiding loss.

One obvious advantage of microstructured fibres with large d/Λ is the low waveguiding loss at a small number of rings. The dispersion characteristics of such fibres can be tuned in a wide range by varying the length scale of the structure. Figure 3 shows the dispersion curves calculated for two-ring fibres with $d_{1,2}/\Lambda = 0.9$ in both rings. The dispersion characteristic of the microstructured fibres considerably shifts to longer wavelengths with an increase in the length scale of the structure (proportional increase in d and Λ, with d/Λ unchanged). To bring the dispersion zero from the range 1.4–1.5 μm, which is commonly used for supercontinuum generation under erbium laser pumping, to 2 μm, the length scale of the structure should be increased by a factor of 3. This is accompanied by an increase in the effective area of the fundamental mode, $A_{\rm eff}$, reducing the nonlinearity coefficient $\gamma = 2\pi n_2/(\lambda A_{\rm eff})$. At $\Lambda = 2$ μm, the zero dispersion wavelength is $\lambda_0 = 1.39$ μm and the effective mode area is $A_{\rm eff} = 2.5$ μm^2 (Fig. 4). At $\Lambda = 6$ μm, we have $\lambda_0 = 1.94$ μm and $A_{\rm eff} \sim 20$ μm^2, and γ is a factor of 8 smaller than that with zero dispersion in the range 1.4–1.5 μm. At the same time, the dispersion slope near $\lambda_0 = 2$ μm ($S = 0.14$ ps nm^{-2} km^{-1}) is smaller than that in the range 1.4–1.5 μm. In particular, $S = 0.53$ ps nm^{-2} km^{-1} at $\lambda_0 = 1.39$ μm. At a zero dispersion wavelength near 2 μm, the effect of fibre diameter on the dispersion curve is also weaker. Figure 5 demonstrates that a change in fibre diameter by ±5% shifts the dispersion zero by no more than ~40 nm at $\lambda_0 = 1.95$ μm ($\Lambda = 6$ μm) and by 106 nm at $\lambda_0 = 1.39$ μm ($\Lambda = 2$ μm).

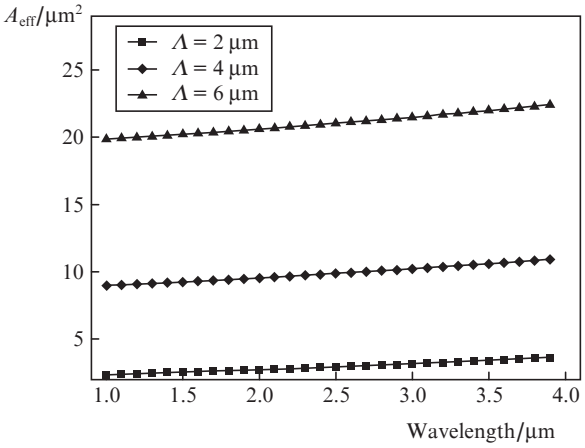

Figure 4. Effective mode area $A_{\rm eff}$ as a function of wavelength for microstructured tellurite glass fibres with $d_{1,2}/\Lambda = 0.9$ and different hole pitches.

The dispersion characteristic of microstructured fibres with $d_{1,2,3}/\Lambda = 0.4$ in the first three rings of holes may have two (or more) zeros in the range 1.5–4 μm (Fig. 6). In comparison with the above two-ring fibre structure, the zero dispersion wavelength reaches 2 μm at a smaller length scale of the structure. The maximum dispersion in the entire spectral range is also lower. As seen in Fig. 6, the dispersion curve at $\Lambda = 2$ μm has two zeros ($\lambda_0 = 1.7$ and 3.7 μm), with the strongest anomalous dispersion of 56 ps nm^{-1} km^{-1}. At $\Lambda = 3$ μm, the dispersion has one zero ($\lambda_0 = 1.9$ μm), like in the case of

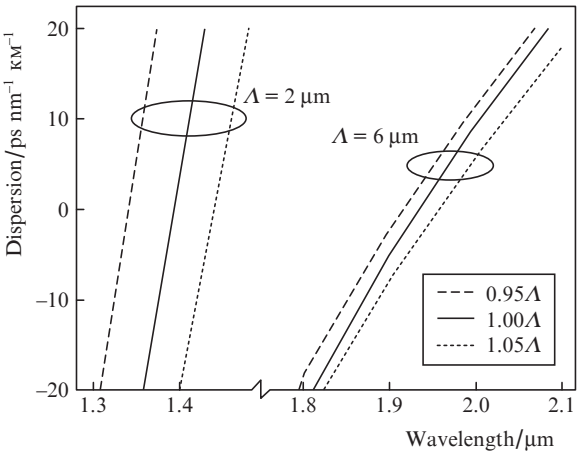

Figure 5. Shift of the dispersion zero in response to a change in hole pitch by ±5% for two-ring microstructured fibres ($d_{1,2}/\Lambda = 0.9$) with a dispersion zero near 1.5 and 2 μm.

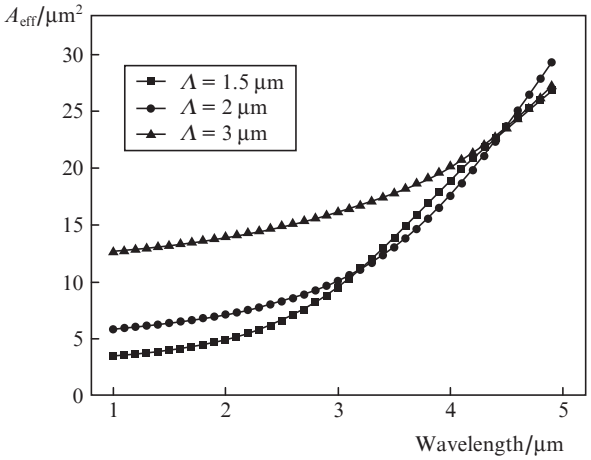

Figure 7. Effective mode area A_{eff} as a function of wavelength for four-ring microstructured tellurite fibres with different hole pitches.

two rings of holes, but the slope of the curve near the dispersion zero is lower: $S = 0.07$ ps nm^{-2} km^{-1}. A specific feature of such fibres is a stronger influence of wavelength on the effective mode area and optical loss. Figure 7 demonstrates that, at Λ = 2 μm, increasing the wavelength from 1 to 4.9 μm increases A_{eff} from 5.9 to 29 μm^2. This is accompanied by a marked increase in loss (to above 1 dB m^{-1}) at wavelengths above 4 μm (Fig. 8), which reduces the advantages related to the larger nonlinear optical coefficient γ near 2 μm in comparison with the two-ring fibre.

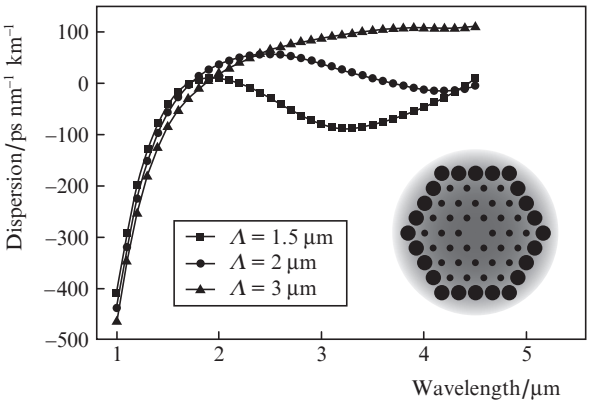

Figure 6. Dispersion profiles of microstructured $68TeO_2$–$22WO_3$–$8La_2O_3$–$2Bi_2O_3$ fibres having four hexagonal rings of air holes with $d_{1,2,3}/\Lambda = 0.4$, $d_4/\Lambda = 0.9$ and different hole pitches.

One important advantage of the four-ring fibre structure, crucial for supercontinuum generation, is the possibility to obtain a flat dispersion profile with two zeros in the range 1.5–4 μm by adjusting the $d_{1,2,3}/\Lambda$ ratio. In particular, recent work [17–19] has shown that, if there are two dispersion zeros, the supercontinuum generation band can be markedly extended owing to the generation of dispersive waves in the normal dispersion region near the zeros. The mechanism of dispersive wave generation in microstructured fibres has been studied in sufficient detail. Under pumping with femtosecond pulses at a wavelength from the anomalous dispersion region near the first zero, supercontinuum generation begins with the formation of a higher order soliton. Because of the disturbances associated with higher order nonlinearities (self-steepening and Raman scattering effects), the soliton breaks up into fundamental solitons, which propagate through the fibre with different group velocities and experience a shift to longer wavelengths. Moreover, the higher order dispersion causes the soliton spectrum to break up into a soliton part and dispersive waves. The spectral position of a dispersive wave can be found from the phase matching condition [15]

$$\Delta\beta = \beta(\omega_P) - \beta(\omega_{DW}) = \sum_{n\geqslant 2} \frac{\beta_n(\omega_P)}{n!}(\omega_{DW} - \omega_P)^n \simeq 0, \quad (4)$$

where $\beta(\omega_P)$ and $\beta(\omega_{DW})$ are the propagation constants at the angular frequencies of the pump source (ω_P) and dispersive wave (ω_{DW}), respectively, and $\beta_n(\omega_P)$ are the coefficients of the Taylor expansion of the propagation constant β about ω_P.

The number of ω_{DW} solutions to Eqn (4) corresponds to the number of zeros in the second-order dispersion curve, and solutions exist at any pump wavelength from the anomalous dispersion region between the zeros. If there is one dispersion

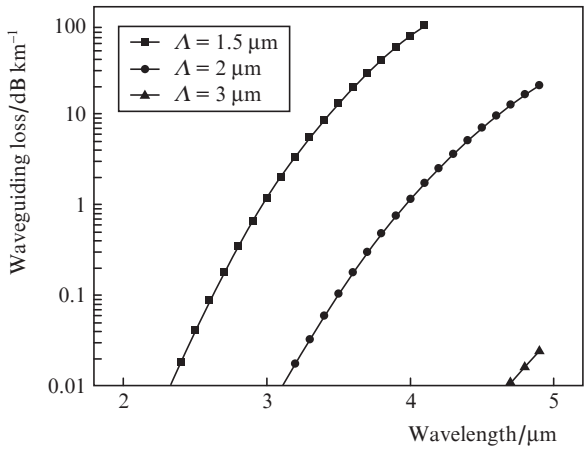

Figure 8. Waveguiding loss as a function of wavelength for four-ring microstructured tellurite fibres with different hole pitches.

zero, an estimate from condition (4) is only possible for the short-wavelength edge of the supercontinuum. The long-wavelength edge is then determined by the Raman shift and soliton damping due to losses in the fibre and, to estimate it, a complete solution to the Schrödinger equation with particular pump pulse parameters is needed. When there are two dispersion zeros, condition (4) for a particular wavelength can be used to estimate the maximum supercontinuum bandwidth, which is governed by the generation of dispersive waves in the normal dispersion regime. Note, however, that effective energy transfer from the pump wave to dispersive waves (and, accordingly, amplification of these latter) can only take place when there is a significant overlap of the soliton spectrum with a dispersive wave, so the actual supercontinuum bandwidth depends on the pump pulse power and duration.

Figure 9 illustrates the effect of pump wavelength, λ_P, on the wavelength of dispersive waves, λ_{DW}, calculated from condition (4) for regions near the first and second dispersion zeros of a fibre with $d_{1,2,3}/\Lambda = 0.4$, $d_4/\Lambda = 0.9$ and $\Lambda = 2$ μm [curves (*1*, *2*)]. In the calculation, we used the first 15 coefficients of the Taylor expansion of the propagation constant β. At a pump wavelength of 1.95 μm, near the shorter wavelength dispersion zero (λ_0 = 1.7 μm), dispersive waves are amplified at $\lambda_{DW1} = 1.38$ μm. Owing to the Raman shift of the soliton in the fibre, the pump energy is transferred to the region of the second zero (λ_0 = 3.7 μm), where, at a soliton wavelength $\lambda_P = 3.25$ μm, the dispersive wave is amplified at $\lambda_{DW2} = 4.92$ μm. The estimated maximum possible supercontinuum bandwidth for this fibre is 3.5 μm. It is worth noting that, because dispersive wave calculations were made only within the spectral range 0.9–5.45 μm, where the refractive index had been measured, the experimentally determined supercontinuum bandwidth may be greater. Curve (*3*) in Fig. 9 represents the estimated short-wavelength edge of the supercontinuum for a two-ring fibre having one dispersion zero ($\lambda_0 = 1.93$ μm). At a pump wavelength $\lambda_P = 1.95$ μm, the phase matching condition is fulfilled at $\lambda_{DW1} = 1.9$ μm. Increasing the soliton wavelength to 2.65 μm shifts the short-wavelength edge of the supercontinuum to $\lambda_{DW1} = 1.06$ μm.

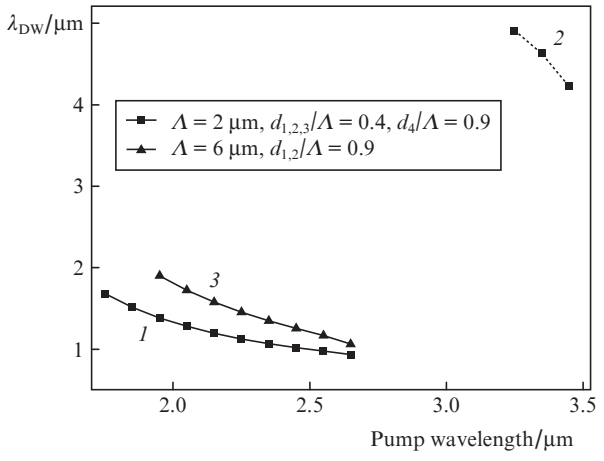

Figure 9. Effect of pump wavelength, λ_P, on the wavelength of dispersive waves, λ_{DW}, calculated from the phase matching condition (4) for (*1*, *2*) a four-ring microstructured fibre having two dispersion zeros and (*3*) a two-ring fibre having one dispersion zero in the range 1–4 μm.

5. Conclusions

High-purity tellurite glass of composition $68TeO_2–22WO_3–8La_2O_3–2Bi_2O_3$ with a net content of regulated 3d transition metal impurities (Fe, Ni, Co, Cu, Mn, Cr and V) within 0.8 ppm by weight has been prepared for the first time. The volume absorption coefficient of the glass at 1.975 μm is 45 dB km^{-1}. The addition of a chemical reagent to the molten glass batch made it possible to substantially reduce the concentration of OH groups in the glass and to obtain an absorption coefficient at ~3 μm as low as ~0.001 cm^{-1}. To our knowledge, this is the lowest absorption coefficient reported to date for OH groups in tellurite glasses.

Precision refractive index measurements throughout the transmission window of the glass (0.9–5.45 μm) enabled a comparative analysis of the dispersion and guidance properties of microstructured fibres of this glass for two fibre geometries attractive for supercontinuum generation at a pump wavelength in the 2-μm range. Both geometries enable the dispersion zero to be shifted to the range 1.7–2 μm. The fibre having two rings of air holes with a large relative diameter offers the advantages of simpler design, low waveguiding losses and weaker wavelength dependence of the effective mode area. At the same time, the fibre with four rings of holes has the potential of lower dispersion values and dispersion slopes throughout the range 1–5 μm. At a pump wavelength near 2 μm, the supercontinuum bandwidth in such fibres may reach at least 3.5 μm.

Acknowledgements. This work was supported by the Presidium of the Russian Academy of Sciences (Programme No. P-2: Novel Optical Materials) and the Russian Foundation for Basic Research (Grant No. 09-02-01124a).

References

1. Sae-Hoon K., Yoko T., Sakka S. *J. Am. Ceram. Soc.*, **76**, 2486 (1993).
2. Sabadel J.C., Armand P., Cachau-Herreillat D., Baldeck P., Doclot O., Ibanez A., Philippot E. *J. Solid State Chem.*, **132**, 411 (1997).
3. Kumar V.V. Ravi Kanth, George A.K., Knight J.C., Russell P.St.J. *Opt. Express*, **11**, 2641 (2003).
4. Feng X., Loh W.H., Flanagan J.C., Camerlingo A., Dasgupta S., Petropoulos P., Horak P., Frampton K.E., White N.M., Price J.H.V., Rutt H.N., Richardson D.J. *Opt. Express*, **16**, 13651 (2008).
5. Domachuk P., Wolchover N.A., Cronin-Golomb M., Wang A., George A.K., Cordeiro C.M.B., Knight J.C., Omenetto F.G. *Opt. Express*, **16**, 7161 (2008).
6. Lin A., Zhang A., Bushong E.J., Toulouse J. *Opt. Express*, **17**, 16716 (2009).
7. Liao M., Chaundhari C., Qin G., Yan X., Suzuki T., Ohishi Y. *Opt. Express*, **17**, 12174 (2009).
8. Liao M., Yan X., Qin G., Chaundhari C., Suzuki T., Ohishi Y. *Opt. Express*, **17**, 15481 (2009).
9. Liao M., Yan X., Qin G., Chaudhari C., Suzuki T., Ohishi Y. *Proc. OFC/NFOEC 2010* (San Diego, CA, USA, 2010) JWA3.
10. Ohishi Y., Qin G., Liao M., Yan X., Suzuki T. *Proc. OFC/NFOEC 2010* (San Diego, CA, USA, 2010) OMG1.
11. Churbanov M.F., Moiseev A.N., Snopatin G.E., Dorofeev V.V., Pimenov V.G., Chilyasov A.V., Lobanov A.S., Kotereva T.V., Plotnichenko V.G., Koltashev V.V., Pyrkov Yu.N. *Phys. Chem. Glasses: Eur. J. Glass Sci. Technol. B*, **49**, 297 (2008).
12. Feng X., Tanabe S., Handa T. *J. Non-Cryst. Solids*, **281**, 48 (2001).
13. Dai S., Zhang J., Yu C., Zhou G., Wang G., Hu L. *Mater. Lett.*, **59**, 2333 (2005).

14. Skilnik L.H., in *Optical Properties of Highly Transparent Solids.* Ed. by S.S. Mitra, B. Bendow (N.Y.–London: Plenum Press, 1975).
15. Plotnichenko V.G., Sysoev V.K., Firsov I.G. *Kvantovaya Elektron.*, **8**, 1495 (1981) [*Sov. J. Quantum Electron.*, **11**, 902 (1981)].
16. Plotnichenko V.G., Nazaryants V.O., Kryukova E.B., Pyrkov Yu.N., Dianov E.M., Galagan B.I., Sverchkov S.E. *Neorg. Mater.*, **45**, 366 (2009).
17. Cristiani I., Tediosi R., Tartara L., Degiorgio V. *Opt. Express*, **12**, 124 (2004).
18. Hilligsoe K.M., Andersen T.V., Paulsen H.N., Nielsen C.K., Molmer K., et al. *Opt. Express*, **12**, 1045 (2004).
19. Gentry G., Lethonen M., Ludvigsen H., Kaivola M. *Opt. Express*, **12**, 3471 (2004).